High proton conduction of organized sulfonated polyimide thin films with planar and bent backbones

Yutaro Ono[†], Ryosuke Goto[‡], Mitsuo Hara[‡],

Shusaku Nagano[‡], Takashi Abe[//], Yuki Nagao[†]*

[†] School of Materials Science, Japan Advanced Institute of Science and Technology, 1-1 Asahidai, Nomi, Ishikawa 923-1292, Japan

[‡] Department of Molecular Design & Engineering, Graduate School of Engineering, Nagoya University, Furo-cho, Chikusa, Nagoya 464-8603, Japan

[§] Nagoya University Venture Business Laboratory, Nagoya University, Furo-cho, Chikusa, Nagoya 464-8603, Japan

// Graduate School of Science and Technology, Niigata University, 8050 Ikarashi 2-no-cho, Nishi-ku, Niigata 950-2181, Japan

*ynagao@jaist.ac.jp (Y.N.), Phone: +81(Japan)-761-51-1541,

Fax: +81(Japan)-761-51-1149, Address: 1-1 Asahidai, Nomi, Ishikawa 923-1292, Japan

Abstract

Fast proton conduction was achieved in organized lamellar structures with in-plane oriented structure parallel to the substrate surface using a lyotropic liquid-crystalline (LC) property. Alkyl sulfonated polyimides (ASPIs) with bent main chain structure were newly synthesized to investigate relations between the higher order structure and proton transport properties. Proton conductivity of all polyimide thin films was greater than 10^{-2} S/cm^{-1}. Grazing-incidence small-angle X-ray scattering (GI-SAXS) revealed that both planar and bent ASPI thin films exhibited humidity-induced lyotropic lamellar structure. Infrared p-polarized multiple-angle incidence resolution (pMAIR) studies revealed that main chain backbones of both planar and bent ASPI thin films show an in-plane orientation parallel to the substrate surface. Results demonstrate that sulfonated alkyl side chains contribute strongly to the lyotropic LC property, which enhances molecular orderings and proton conductivity by water uptake. This study extends knowledge of the molecular design for highly proton conductive polymers with humidity-induced lyotropic LC property.

1. Introduction

Studies of energy conversion technology have expanded rapidly to support the use of next-generation power sources for sustainable energy. Polymer electrolyte fuel cells have been anticipated as ideal energy conversion systems because they are environmentally friendly and highly efficient systems for conversion from chemical energy to electrical energy. Great effort has been devoted to studies of advanced polymer electrolytes because they are important components of polymer electrolyte fuel cells.[1–5]

To achieve high proton conductivity of polymer electrolytes, various polymer electrolyte membranes such as perfluorosulfonated polymers,[6–9] sulfonated block copolymers and graft copolymers have been examined based on a concept of the well phase-separated hydrophilic channels composed of hydrophobic backbones and hydrophilic parts. The proton conductivity of polymer electrolyte membranes is closely related to several parameters such as acidity, number of sulfonic acid groups, main chain and side chain structures, and membrane morphology.[10–15] From a different perspective, structural confinement effects of polymer electrolyte thin films have been reported.[16–37] Structure and transport properties in confined polymer thin films differ drastically from those of the bulk materials because of interactions between the polymer and substrate surface.[38,39] For example, a study of Nafion thin films demonstrated that the degree of the

phase segregation, water uptake, and proton conductivity decreased concomitantly with decreasing film thickness. [26,34,35]

Recent investigations have assessed structural controls of the proton conductive channels undertaken for the enhancement of proton conductive properties.[19–25] Sato and Matsui *et al.* reported that the well-defined two-dimensional lamellar structure of Langmuir–Blodgett thin films shows high proton conductivity with large anisotropic proton conduction. [19–21] These results demonstrate the possibility of proton conductivity enhancement using the molecular orientation. Additionally, several ion conductive liquid-crystalline (LC) materials have been developed. Furthermore, the relation between molecular assembled nanostructures and transport properties has been studied.[40–49] These materials comprise ionic liquids and thermotropic LC property. These LC materials exhibit interesting properties such as one-dimensional ion transport, switching ionic conductivity, and phase transition.

Our recent study has elucidated that proton conductivity enhancement originates from the molecular ordering and orientation of the LC-like domains of alkyl sulfonated polyimide (ASPI) thin films.[22–24] Actually, ASPI exhibits a lyotropic LC property by water uptake because of their rigid aromatic backbones and sulfonated alkyl side chains holding an amphiphilic property. ASPI thin films with rigid and planar molecular

structure show a lamellar structure parallel to the substrate surface, which expands reversibly to the out-of-plane direction by water uptake. Furthermore, the degree of the molecular ordering improves by water uptake. The proton conductivity improves by these structural changes and exhibits more than 10^{-2} S/cm.[22–24] Nevertheless, the role of backbone rigidity and the side chain contribution for the lyotropic LC property remains unclear.

Ando and co-workers have investigated details of molecular aggregation structures of both fully aromatic and semialiphatic polyimides with no sulfonated alkyl side chains.[50] They found that the polyimide consisting of pyromellitic dianhydride and 4,4-diaminodiphenyl ether with nonplanar and bent molecular structure includes a mixture of the amorphous matrix and LC-like ordered domains. Steric effects of the polyimide have influenced the interchain packing structure. In other words, different monomer structures can modify such higher order structures of polyimides.

This work provides new insight into the relation between the proton transport property and organized polymer nanostructure. Herein, we synthesized four humidity-induced lyotropic LC polyimides consisting of planar and bent polymer backbones with alkyl sulfonated side chains. The origin of lyotropic LC property in ASPI thin films was elucidated from the viewpoint of main chain rigidity and side chain effects. Grazing-

incidence small-angle X-ray scattering (GI-SAXS) was used to elucidate the organized structure of thin films. In addition, infrared p-polarized multiple-angle incidence resolution (pMAIR) studies were conducted to reveal a molecular orientation to the substrate surface. AC impedance and water uptake by quartz crystal microbalance (QCM) were measured to quantify the proton conductivity. Both planar and bent ASPI thin films exhibited high proton conductivity and humidity-induced lyotropic lamellar structure parallel to the substrate plane. This study extends the molecular design for highly proton conductive polymers with humidity-induced lyotropic LC property.

2. Experimental section

2-1. Materials

1,4,5,8-Naphthalenetetracarboxylic dianhydride (NTDA) was used as received from Sigma–Aldrich. 3,3′-Dihydroxybenzidine, 1,3-propanesultone, pyromellitic dianhydride (PMDA), 4,4'-oxydiphthalic dianhydride (ODPA), and 4,4'-biphthalic dianhydride (BPDA) were used as received from TCI, Japan. Sodium hydroxide (Kishida Chemical Co. Ltd., Japan), hydrochloric acid (Nacalai Tesque Inc., Japan), *m*-cresol, and triethylamine (TEA) (Kanto Chemical Co. Inc., Japan) were used as received. Acetic acid, acetic anhydride, methanol, and acetone were obtained from Wako Pure Chemical

Industries Ltd., Japan. 3,3'-Bis(sulfopropoxy)-4,4'-diaminobiphenyl (BSPA) was synthesized according to previous reports[22–24] (Scheme S1, Figure S1).

Sulfonated polyimide with various molecular structures was prepared using the same polymerization scheme (Scheme 1). A typical synthesis for ASPI is described as presented below. 1 mmol of BSPA, 1 mmol of anhydride-monomer, 7 ml of m-cresol, and 300 µl of TEA were added to a round-bottom flask equipped with a magnetic stirrer bar under argon atmosphere at a constant temperature of 150°C for 6 h. The polymerized product was precipitated in large excess cooled acetone. The precipitate was collected by centrifuge, washed several times with fresh acetone, and dried under vacuum overnight. The final product was subjected to an ion-exchange process using Amberlyst. ^{1}H NMR measurements were taken using a spectrometer (Bruker Avance III 400; Bruker Analytik GmbH) using deuterated dimethyl sulfoxide used and tetramethylsilane (TMS). Infrared (IR) attenuated total reflection (ATR) spectra were measured with a Fourier-transform infrared (FTIR) spectrometer (Nicolet 6700; Thermo Fisher Scientific Inc.) in the range of 400−4000 cm^{-1}.

The chemical structures of the synthesized ASPI by ^{1}H NMR are presented in Figure S2. Peaks between δ = 7 to 9 ppm corresponded to the H atoms in the aromatic rings. The aliphatic protons were observed at δ = 2.0−4.4 ppm. Integration of proton peaks in ^{1}H

NMR spectrum showed good agreement with the number of hydrogens in both the backbone and side chain of ASPI structure. No residual amide or carboxylic protons were noticed, which indicates that the imidization reaction was complete. The spectrum was observed after ion exchanged product: an extremely small amount of the TEA was observed. The calculated residual TEA was almost 1%. The calculated ion exchange capacity (IEC) values were estimated to be 2.86 (ASPI-1), 3.08 (ASPI-2), 2.69 (ASPI-3) and 2.75 mequiv g^{-1} (ASPI-4) by ^{1}H NMR results. The yields of each polymer were 80% (ASPI-1), 63% (ASPI-2), 68% (ASPI-3), and 85% (ASPI-4). FTIR-ATR spectra of all ASPIs are presented in Figure S3. The absorption bands of the (C=O) were observed at 1720 and 1780 cm^{-1}, which can be attributable as C=O asymmetric and symmetric stretching vibrations in ASPI-2, ASPI-3, and ASPI-4 cases. Similar vibrations of the C=O were observed at 1660 and 1710 cm^{-1} in ASPI-1. The observed vibrational mode at 1500 cm^{-1} is attributed to the phenyl C−C stretching vibration. The vibrational mode at 1380 (in ASPI-2, ASPI-3, ASPI-4) and 1350 (in ASPI-1) cm^{-1} is a C−N bond of the imide groups. The characteristic absorption bands of the sulfonic acid groups (O=S=O) normally appeared between 1030 cm^{-1} and 1250 cm^{-1}. The molecular weights (Mw) of ASPI were ascertained using gel permeation chromatography (GPC). This study selected high molecular weight (ca. 5–8 $\times 10^{5}$) ASPI samples.

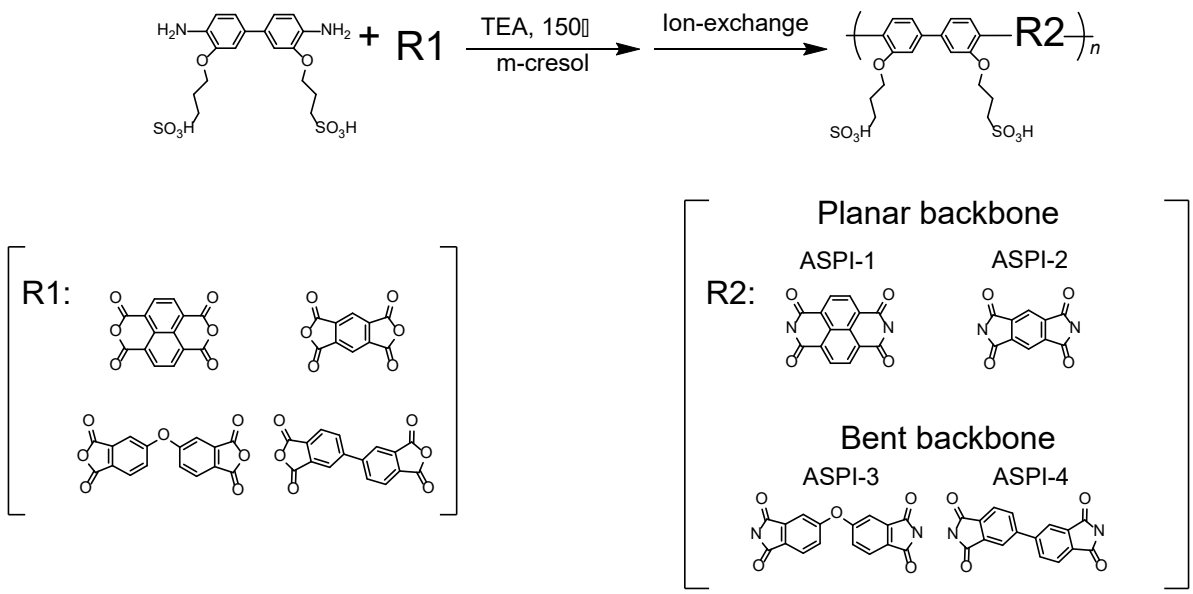

Scheme 1. Synthesis of sulfonated polyimide.

2-2. Gel Permeation Chromatography (GPC)

The molecular weights of ASPI were found using GPC (LC-2000plus; Jasco Corp.) with Shodex GF-1G 7B and GF-7M HG columns. An eluent was applied at a flow rate of 1.0 mL min^{-1} using mixture of DMF, H_2O, CH_3COOH, and $NaNO_3$. Before injection of the sample into the column, solutions were filtered through a 0.50 μmϕ PTFE hydrophobic filter. Polystyrene was used as a standard sample for molecular weight.

2-3. Thin Film Preparation

For this study, Si, SiO_2 substrates (each 15 × 15 × 0.5 mm) and SiO_2 -coated 9 MHz quartz crystal microbalance (QCM) substrates (Seiko EG&G Co. Ltd.) were used respectively for thin films using spin-coating (ACT-200; Active Co. Ltd.), few wt% ASPI dispersion was used. Thicknesses of ca. 500 nm were found using an atomic force microscope (AFM, VN-8000; Keyence Co.) and a White interference microscope (BW-S506; Nikon Corp.). The ASPI thin films were dried for 12 hr in a desiccator.

2-4. Proton Conductivity Measurement of ASPI Thin Films

The proton conductivity of thin films was obtained by impedance analyzer and dielectric interface system (SI1260 and SI1296; Solartron Analytical). Impedance data were collected in the frequency range between 10 MHz and 1 Hz with amplitude of 50 mV. A humidity-controlled and temperature-controlled chamber (SH-221; Espec Corp.) was used for a relative humidity (RH) range of 40–95% at 298 K. The direction of impedance measurement was taken parallel to the substrate (in-plane direction). The gold electrodes were prepared at two parallel edges of thin film by the gold paste. Each impedance value was plotted after the obtained semi-circle did not change in each humidity. Proton conductivity (σ) was calculated as following definition,

$$\sigma = \frac{d}{Rlt}, \quad (1)$$

where R denotes the resistance value from impedance, l and t stand for the contact electrode length and the film thickness, respectively, and d represents the distance between the gold electrodes.

2-5. Water Uptake Measurements

Water uptake was measured using an *in-situ* QCM system. QCM substrates were connected to an oscillation circuit with a DC power supply and a frequency counter (53131A; Agilent Technologies Japan Ltd.). The QCM substrate was placed in an in-house constructed humidity chamber with a high-resolution RH sensor. Various humidity environments were produced using dry N_2 and humidified streams applied by a humidity controller (BEL Flow; BEL Japan Inc.). The frequencies before and after spin-coating of the QCM substrate were confirmed at the dry N_2 stream for determination of the mass of dry film using the Sauerbrey equation

$$\Delta m = \frac{S \times \sqrt{\rho \mu}}{2 \times F^2} \times (-\Delta F), \quad (2)$$

where S represents the electrode surface area, ρ *and* μ denote the quartz density and quartz shear modulus, and F stands for the fundamental frequency of QCM substrate.

The water content λ was calculated as

$$\lambda = \left(\frac{m}{m_0} - 1\right) \times \frac{EW}{M_{H_2O}} \quad , (3)$$

where m signifies the film mass at each RH, m_0 stands for the film mass at the 0%RH, M_{H_2O} denotes the molecular mass of water molecular, and EW expresses the equivalent weight of each ASPI.

2-6. Polarized Optical Microscopy (POM)

POM was used to elucidate the lyotropic LC-like domain morphologies and their size in ASPI films. The POM observations were taken using an optical microscope (BX51, BX51-P; Olympus Corp.) with a digital camera (DP28 camera; Olympus Corp.) All POM observations were conducted at room temperature and ambient humidity.

2-7. Grazing-Incidence Small-Angle X-ray Scattering (GI-SAXS) Measurements

In-situ GI-SAXS was performed on a X-ray diffractometer (FR-E; Rigaku Corp.) with an R-AXIS IV two-dimensional detector. The thin film sample was placed into the humidity-controlled cell on the goniometer and vertical stage (ATS-C316-EM/ALV-300-HM; Chuo Precision Industrial Co. Ltd.). The humidified cell holds Kapton windows. To control the humidity nitrogen gas was used from the gas cylinder without further dehumidification.

Wavelength and beam size of X-ray were λ = 0.1542 nm by Cu Kα radiation and approximately 300 μm × 300 μm, respectively. The camera length was 300 mm and the incidence angle was set in the range of 0.20° to 0.22°.

2-8. Infrared p-polarized Multiple-angle Incidence Resolution Spectrometry (pMAIRS)

pMAIRS which was developed by Hasegawa[51-54] was carried out to identfy IP and OP molecular vibrations in an identical thin film. An FT-IR spectrometer (Nicolet 6700; Thermo Fisher Scientific Inc.) was used for pMAIRS measurements equipped with a mercury–cadmium–telluride (MCT) detector. P-polarized light was used by a ZnSe polarizer. The angles of incidence for single-beam spectra were taken from 38° through 8° in 6° steps. The wavenumber resolution and number of scans were 4 cm^{-1} and 64 times for each incident angle, respectively. Dry air or N_2 gases were purged through the sample compartment and inside of the spectrometer to achieve less than 5% for humidity condition. The aperture was fully opened to obtain wide range beam size. A metal plate with small pore arrays was placed in the light path to avoid the light saturation for the MCT detector. The pMAIRS analysis from the angular dependent spectra was conducted automatically using pMAIRS analyzer software (Thermo Fisher Scientific Inc.).

3. Results and Discussion

3-1. Proton Conductivity and Water Uptake

The proton conductivity of the planar ASPI-1, ASPI-2, bent ASPI-3, and ASPI-4 thin films for various RH at 298 K is presented in Figure 1. Proton conductivity of all ASPI thin films increased exponentially with RH, which is a typical phenomenon of proton conductive polymers. Proton conductivity for all ASPI thin films showed a remarkably higher value above 10^{-2} S / cm (at 25°C, 95% RH). This value is higher than that of 400-nm-thick Nafion thin film,[18] which indicates that not only planar ASPI but also bent ASPI thin films can exhibit high proton conductivity as a form of thin film.

The water uptake of the polymer electrolyte membrane is an important factor for the proton conductivity. The RH dependence of water uptake of planar ASPI-1, ASPI-2, bent ASPI-3, and ASPI-4 thin films was investigated for hydration behavior using *in-situ* QCM measurements. The obtained data are presented in Table 1. Figure S4 presents the humidity dependence of the number of water molecules per sulfonic acid (λ [H_2O / SO_3H]). All ASPI thin films showed similar curves for water uptake.

As presented in Figure 2, the proton conductivity of the planar ASPI-1 and ASPI-2 exhibits more than two times higher conductivity than that of the bent ASPI-3 and ASPI-

4 in the high water uptake condition. An earlier study demonstrated that the degree of molecular ordering strongly affects proton conductivity.[24] To reveal the origin for the high proton conductivity in both planar and bent ASPI thin films, POM, GISAXS, pMAIR measurements were carried out.

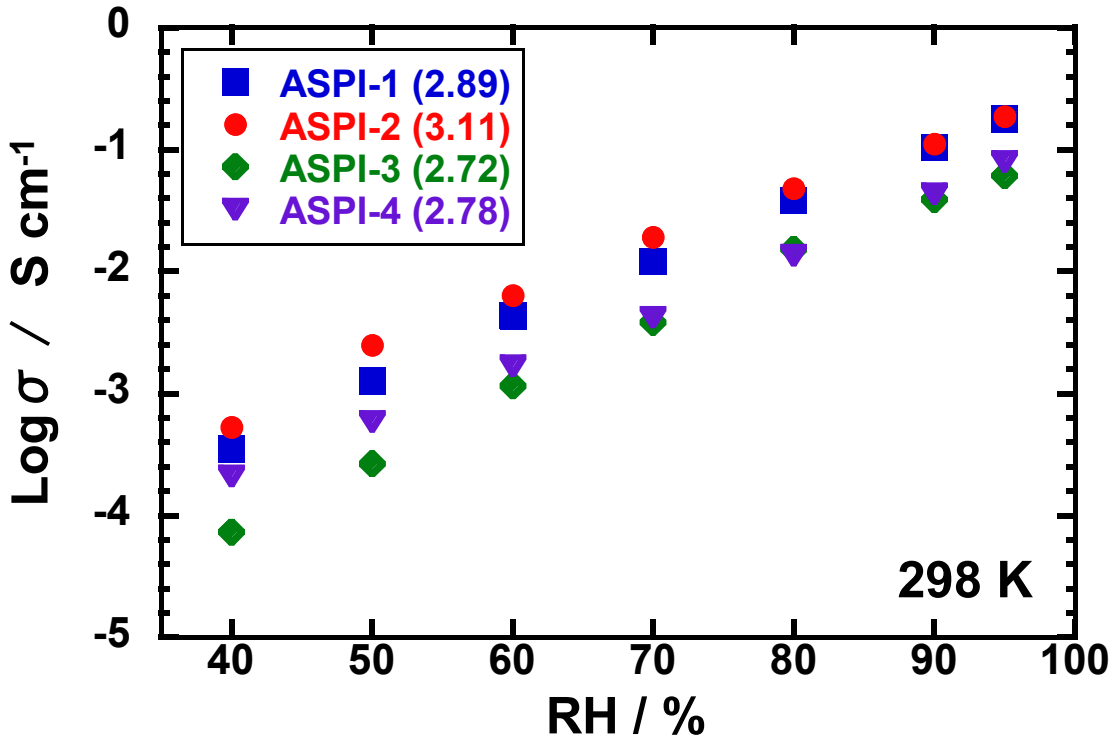

Figure 1. Proton conductivity of the ASPI-1 (IEC = 2.89), ASPI-2 (IEC = 3.11), ASPI-3 (IEC = 2.72), and ASPI-4 (IEC = 2.78) thin films as a function of relative humidity at 298 K.

Table 1. Physical Properties of ASPI thin films.

Sample	IEC (mequiv/g)	Mw	H^+ conductivity[c] (S/cm)	Water uptake[d] (%)	λ^d
ASPI-1	2.89[a]	4.9×10^5	1.78×10^{-1}	76.8	14.8

	(2.86)[b]				
ASPI-2	3.11[a] (3.08)[b]	8.0×10^5	1.96×10^{-1}	78.7	14.0
ASPI-3	2.72[a] (2.69)[b]	6.5×10^5	0.29×10^{-1}	63.3	12.9
ASPI-4	2.78[a] (2.75)[b]	5.6×10^5	0.80×10^{-1}	66.0	13.3

[a] Calculated from chemical structure. [b] Calculated from ^{1}H NMR results. [c] Proton conductivity, [d] water uptake, and λ were measured at 95% RH.

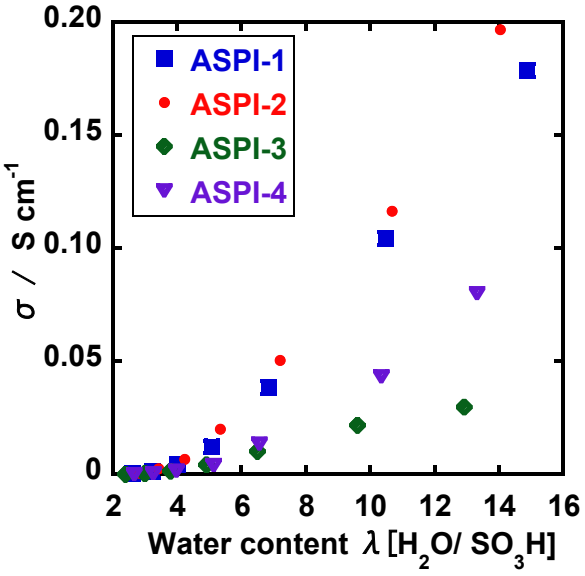

Figure 2. Proton conductivity of the ASPI thin films as a function of the λ value.

3-2. Morphology

Figure 3 portrays representative POM images of the planar ASPI-1, ASPI-2, bent ASPI-3, and ASPI-4 thin films. All ASPI films exhibited strong birefringence, which can be attributed to LC-like morphology. Our previous study revealed that the molecular weight of polymer affects the LC optical domain size[24] Therefore in this study, similar molecular

weight (Table 1) was chosen for planar and bent ASPIs for comparison. Results suggest that the LC-like morphology and domain size depend not only on the molecular weight but also the polymer backbone. Differences of the morphology and domain size can affect the internal nanostructure. Therefore, detailed structural analysis was conducted using GI-SAXS measurements.

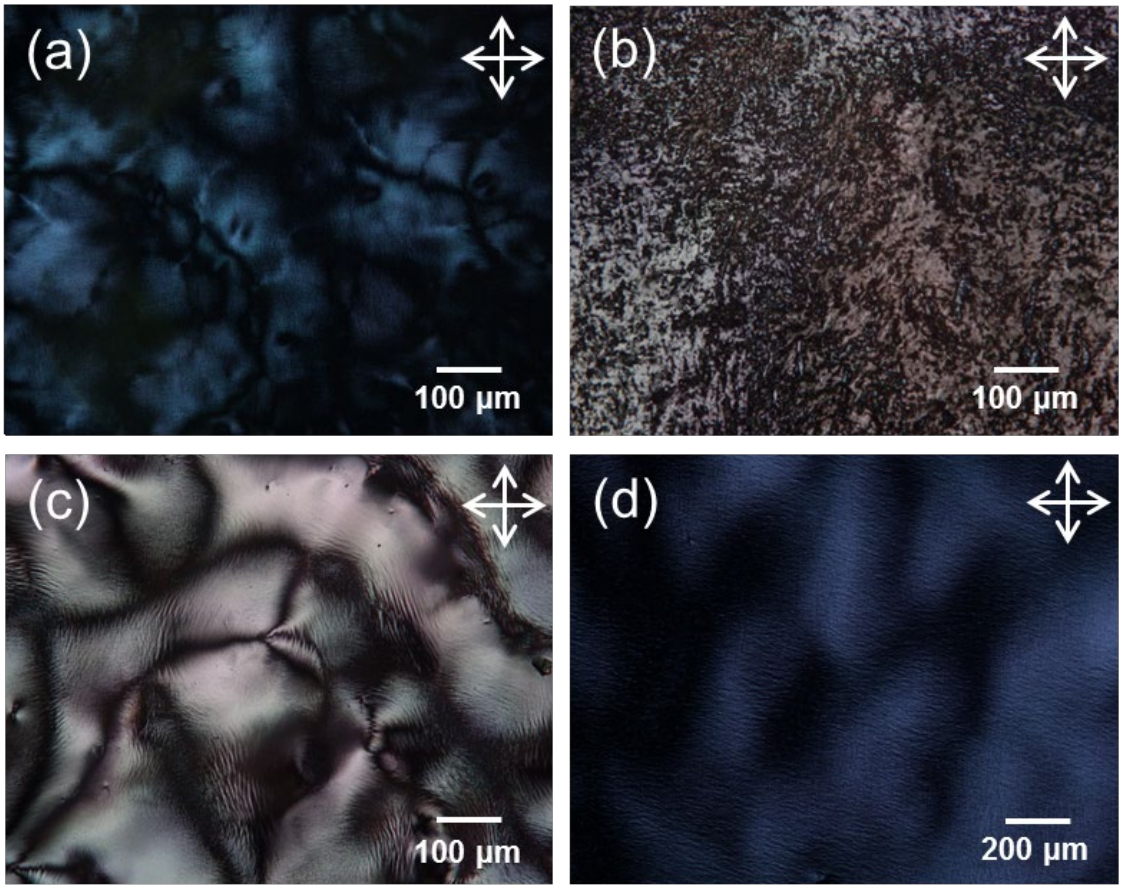

Figure 3. Polarized optical microscope image of the ASPI thin films: (a) ASPI-1, (b) ASPI-2, (c) ASPI-3, and (d) ASPI-4

3-3. GI-SAXS

To investigate the molecular ordered structure at the various humidity conditions, *in-situ* GI-SAXS measurements were taken for planar ASPI-1, ASPI-2, bent ASPI-3, and ASPI-4 thin films. Figure 4 portrays 2D GI-SAXS patterns at 0 and 95% RH and λ value dependent 1D GI-SAXS profiles in the in-plane (IP) and out-of-plane (OP) directions. In our previous study of the GI-SAXS measurements (Figure 4b), a self-assembled lamellar structure parallel to the substrate surface has been determined in the planar ASPI-2 thin film.[22,24] This lamellar distance expands linearly to the out-of-plane direction by water uptake. Furthermore, molecular ordering improves by water uptake based on the lyotropic LC property (Figure S5). In the in-plane direction, an uptaken water insensitive scattering peak (q_y = 0.38 Å^{-1}) is visible, which is attributable to the periodic monomer unit length.

The planar ASPI-1 (Figure 4a), bent ASPI-3 (Figure 4c), and ASPI-4 (Figure 4d) thin films exhibit a similar humidity-dependent self-assembly structure. The d-spacing and assignment of the peaks are presented in Table 2. Figures 5 and 6 respectively depict similar behavior for enhancement of the molecular ordering and linear expansion of lamellar structure by water uptake, which is visible for all ASPI thin films. In the planar structure of ASPI-1, π-stacking at q_y = 1.75 Å^{-1} (d = 0.35 nm) was observed because of the strong interaction of the aromatic ring. This scattering peak was enhanced by water uptake.

In the in-plane direction at q_y = 0.38 Å^{-1} (d=1.63 nm), the peak for periodic monomer unit length of the polyimide main chain was observed only in the planar-backbone ASPI-1 and ASPI-2 thin films. This value was found to be close to the periodic unit length estimated from DFT calculation. In the cases of the bent ASPI-3 and ASPI-4 thin films, no apparent scattering peak by the periodic monomer unit length was observed. Therefore main chain orderings of the bent ASPI-3 and ASPI-4 parallel to the surface direction are lower than those of the planar ASPI-1 and ASPI-2 thin films. Nevertheless, uptaken water sensitive peaks in the out-of-plane direction were observed as a lamellar structure, indicating a humidity-induced lyotropic lamellar structure parallel to the substrate plane. Ando *et al.* assessed the molecular aggregation structures of polyimides with both aromatic planar and bent molecular structures using GI-SAXS analysis.[50] The aromatic polyimide chains with nonplanar and bent molecular structure are packed laterally along the in-plane direction in ordered domains. However, the degree of molecular ordering in the bent polyimide is weaker than that in the planar polyimide. In the case of ASPI, the amphiphilic polyimide with alkyl sulfonated side chains can promote the organization of the lamellar structure with in-plane orientation because of the lyotropic LC property. Results obtained using GI-SAXS revealed that both planar and bent polymer thin films formed an in-plane oriented lamellar structure in which the lamellar distance expanded to

the out-of-plane direction and the degree of molecular ordering improved by water uptake.

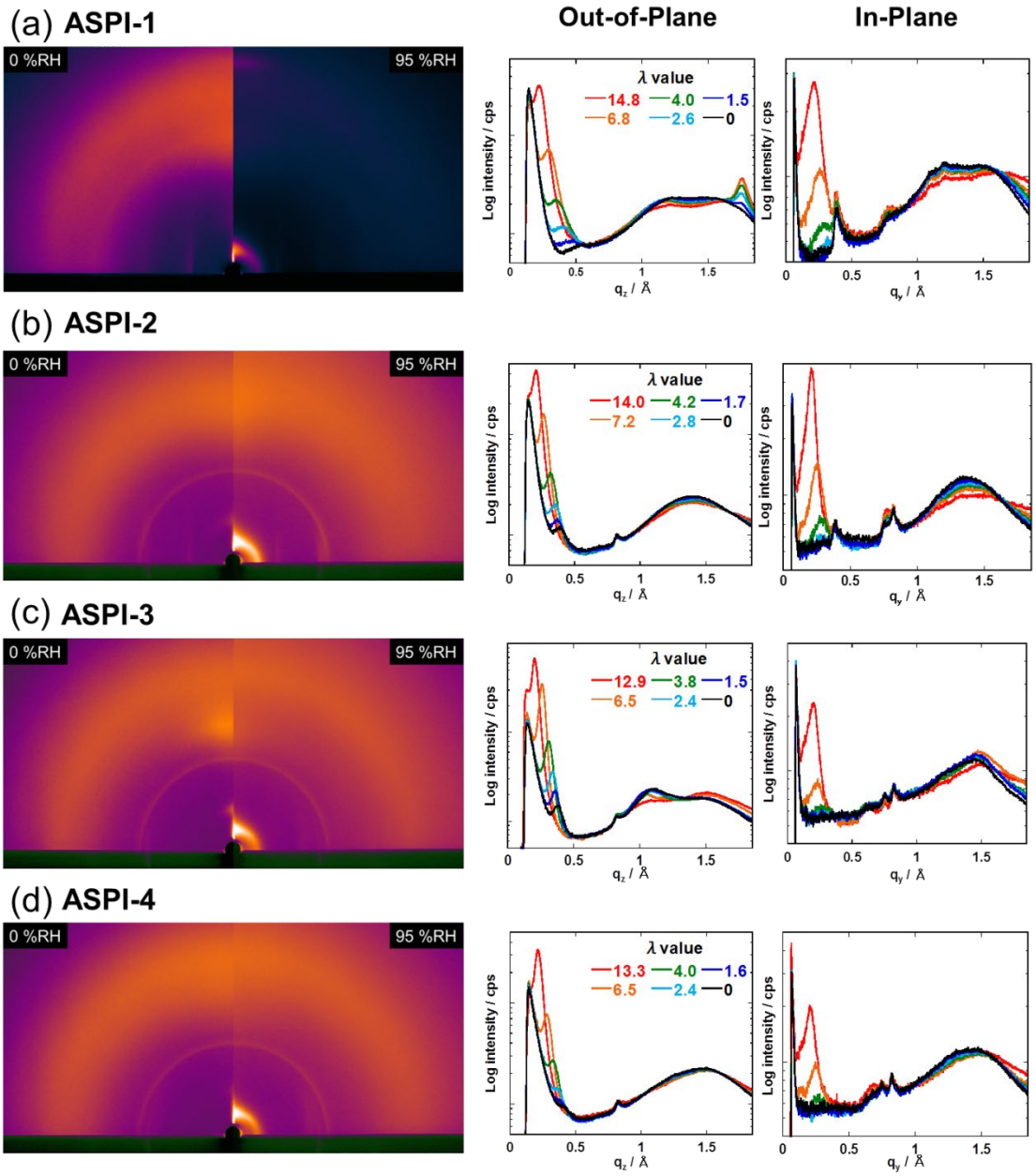

Figure 4. The 2D GI-SAXS patterns at 0%RH and 95%RH respectively, and 1D GI-SAXS profiles in the in-plane and out-of-plane directions as a function of the λ value of the (a) ASPI-1, (b) ASPI-2, (c) ASPI-3, and (d) ASPI-4 thin films. Scattering arcs at the positions of q_y = 0.75 and 0.82 $Å^{-1}$ were originated by diffraction from the window material for the humidity-controlled cell.

Table 2. d-Spacing and assignment in the in-plane (IP) and out-of-plane (OP) directions

Sample	Direction	d-spacing / nm		Assignment
		0% RH	95% RH	
ASPI-1	OP	1.3	2.85	lamellar
	OP	—	0.35	π-stack
	IP	1.6	1.6	(001) Monomer unit length
ASPI-2	OP	1.6	3.0	lamellar
	OP	0.44	0.44	ch-pack
	IP	1.6	1.6	(001) Monomer unit length
ASPI-3	OP	1.66	3.08	lamellar
	OP	0.56	0.58	ch-pack
ASPI-4	OP	1.52	2.94	lamellar
	OP	0.42	0.42	ch-pack

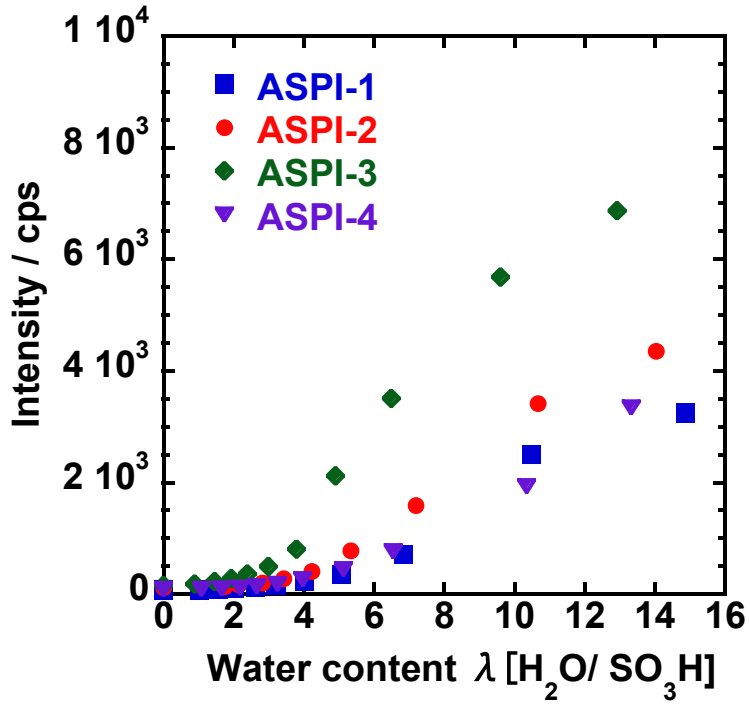

Figure 5. Scattering intensity of the lamellar structure for ASPI-1, ASPI-2, ASPI-3, and ASPI-4 thin films as a function of the λ value.

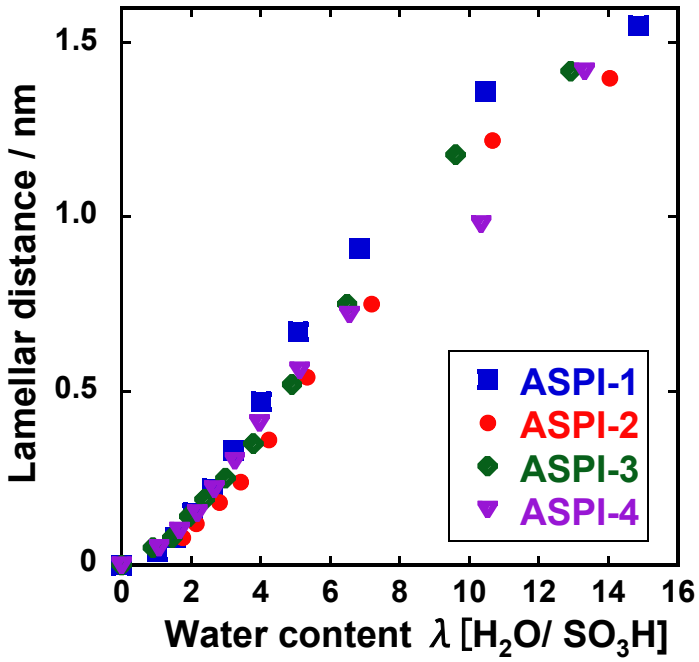

Figure 6. Lamellar distance (Δ*d*-value) as function of the λ value of the ASPI thin films.

3-4. pMAIRS

Infrared p-polarized multiple-angle incidence resolution spectrometry (pMAIRS) was applied to the ASPI thin films to ascertain the orientation of the main chain. IR pMAIRS is increasingly regarded as a powerful spectroscopic tool for investigating molecular orientation in thin films.[51–54] Figure 7 presents pMAIR spectra of the planar ASPI-1, ASPI-2, bent ASPI-3, and ASPI-4 thin films. The observed vibrational modes at 1380 and 1500 cm $^{-1}$ except ASPI-1 are assigned respectively to the C–N bonds of the main chain and to phenyl C–C stretching vibration. Adjacent vibrational modes at 1720 and 1780 cm^{-1} respectively correspond to the C=O asymmetric and symmetric stretching vibrations of imide groups. In a similar manner, pMAIR spectrum of the planar ASPI-1 shows the C–N bonds, C–C stretching vibration, and C=O asymmetric and symmetric stretching vibrations observed respectively at 1350, 1500, 1680, and 1720 cm^{-1}.

The degree of molecular orientation is calculable from in-plane and out-of-plane absorbance for each functional group.[54] A large difference between IP and OP absorbance reflects the anisotropic orientation of the molecular structure. All thin films gave stronger absorbance in the IP spectrum than in the OP spectrum at C=O symmetric and C–N stretching vibrational modes. These vibrational modes correspond to the main chain orientation parallel to the substrate surface. No large differences in molecular orientation

among all ASPI thin films has been confirmed. Both pMAIR and GI-SAXS results show good consistency for in-plane orientated structures of main chains.

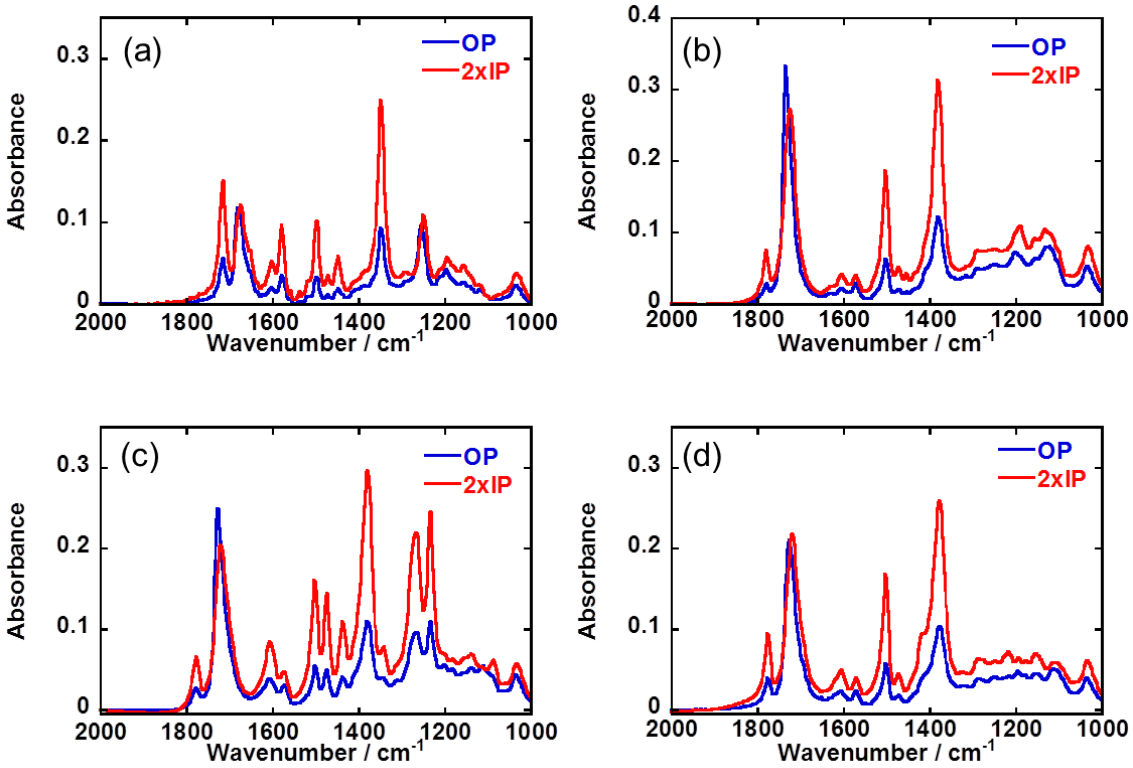

Figure 7. pMAIR spectra of the (a) ASPI-1, (b) ASPI-2, (c) ASPI-3, and (d) ASPI-4 thin films.

3-5. Planar and Bent ASPI Thin Films

From structural analyses conducted using both pMAIRS and GI-SAXS, we propose the organized lamellar structure with highly in-plane ordering structure for high proton conduction as shown in Figure 8. All ASPI thin films enhance the molecular ordering with expansion of lamellar structure to the out-of-plane direction by water uptake. Amphiphilic polyimides with alkyl sulfonated side chains drive the organized lamellar structure with

the in-plane orientation. Results indicate that not only planar but also bent polymer backbones of the ASPI thin films exhibit high proton conductive channels because of the lyotropic LC property. *In-situ* FT-IR results in Figure S6 and S7 reveal that dissociation state of proton at sulfonic acid groups is identical in all ASPI thin films. The difference of proton conductivity between the planar and bent ASPI thin films can be derived from the degree of molecular ordering. Smectic ordering of main chains in ASPI-1 and ASPI-2 thin films can enhance the water uptake in the high RH region and can enable exhibition of higher proton conductivity.

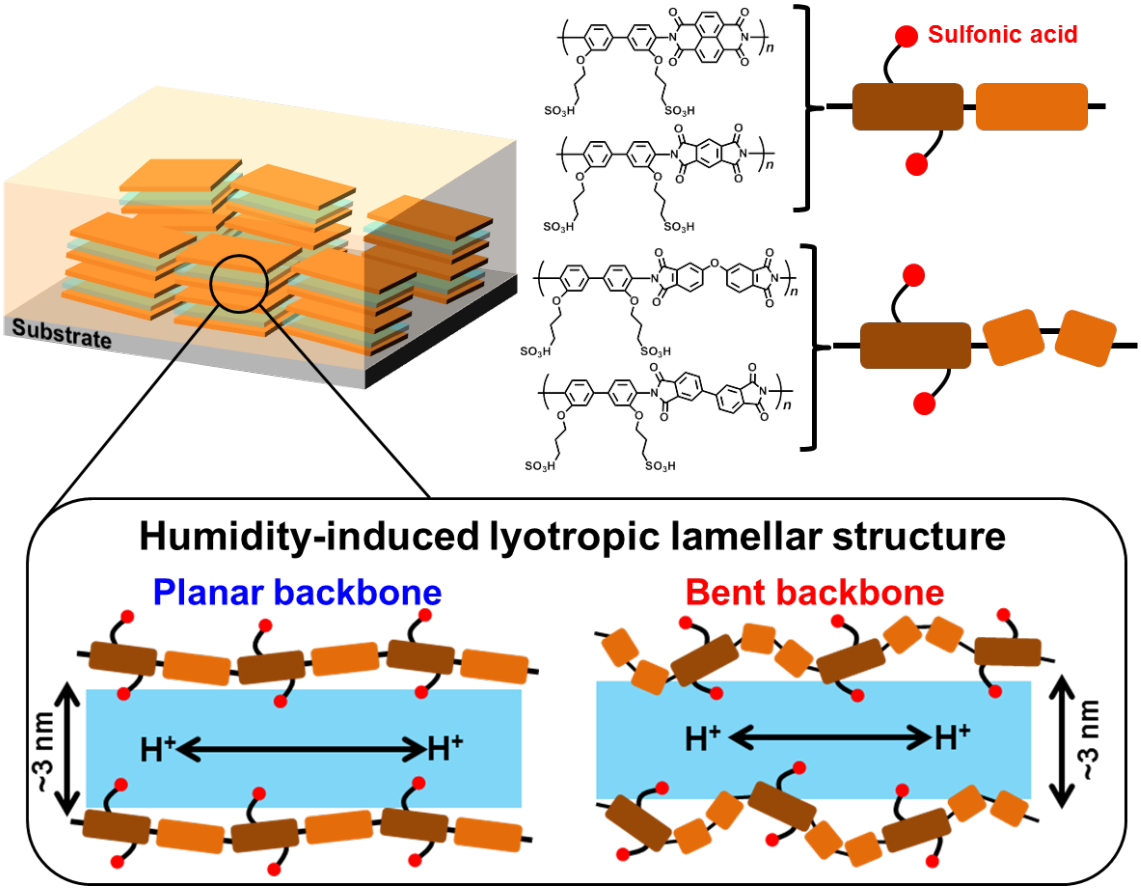

Figure 8. Proposed organized lamellar structure with a highly in-plane ordered structure of both planar and bent polymer backbones.

4. Conclusion

Understanding the relation between structure and proton transport property is fundamentally important to develop high proton conductive materials. In earlier studies, interchain packing for the organized lamellar structure was suppressed by steric effects of nonplanar and bent backbones of polyimides. This study provides a new perspective of the organized lamellar structure using lyotropic LC property by alkyl sulfonated groups at the side chain. Our results indicate that amphiphilic polyimides with alkyl sulfonated

side chains drive the organized lamellar structure with in-plane orientation in both planar and bent backbones. These organized lamellar structures of the in-plane oriented ASPI thin films achieve high proton conductivity exceeding 10^{-2} S/cm. The degree of the molecular ordering of those hydrated domains increased with water uptake. Results obtained through this study extend the molecular design for high proton conductive polymers with humidity-induced lyotropic LC property.

Acknowledgments

This work was supported in part by the Nanotechnology Platform Program (Molecule and Material Synthesis) of the Ministry of Education, Culture, Sports, Science and Technology (MEXT), Japan. This work was partially supported by Iketani Science and Technology Foundation (ISTF), JAPAN.

Supporting information

Synthesis and characterization of sulfonated polyimide, ^{1}H NMR spectra, FT-IR spectra, water solubility test, mechanical test, water uptake, *in-situ* FT-IR spectra, and temperature dependence of proton conductivity.

Author information

Corresponding author

*ynagao@jaist.ac.jp Phone: +81(Japan)-761-51-1541, Fax: +81(Japan)-761-51-1149, Address: 1-1 Asahidai, Nomi, Ishikawa 923-1292, Japan

Notes

The authors have no financial conflict of interest to declare.

References

(1) Li, N.; Guiver, M. D. Ion Transport by Nanochannels in Ion-Containing Aromatic Copolymers. *Macromolecules* **2014**, *47*, 2175–2198.

(2) He, G.; Li, Z.; Zhao, J.; Wang, S.; Wu, H.; Guiver, M. D.; Jiang, Z. Nanostructured Ion-Exchange Membranes for Fuel Cells: Recent Advances and Perspectives. *Adv. Mater.* **2015**, *27*, 5280–5295.

(3) Shin, D. W.; Guiver, M. D.; Lee, Y. M. Hydrocarbon-Based Polymer Electrolyte Membranes: Importance of Morphology on Ion Transport and Membrane Stability. *Chemical Reviews* **2017**, *117*, 2175–2198.

(4) Rikukawa, M.; Sanui, K. Proton-conducting polymer electrolyte membranes based on hydrocarbon polymers. *Prog. Polym. Sci.* **2000**, *25*, 1463–1502.

(5) Miyatake, K.; Bae, B.; Watanabe, M. Fluorene-containing cardo polymers as ion conductive membranes for fuel cells *Polym. Chem.* **2011**, *2*, 1919–1929.

(6) Mauritz, K. A.; Moore, R. B. State of Understanding of Nafion. *Chem. Rev.* **2004**, *104*, 4535–4585.

(7) Schmidt-Rohr, K.; Chen, A. Q. Parallel Cylindrical Water Nanochannels in Nafion Fuel-Cell Membranes. *Nature Mater*. **2008**, *7*, 75–83.

(8) Gebel, G.; Diat, O. Neutron and X-ray Scattering: Suitable tools for Studying Ionomer Membranes. *Fuel Cells* **2005**, *5*, 261–276.

(9) Hsu, W. Y.; Gierke, T. D. Ion Transport and Clustering in Nafion Perfluorinated Membranes. *J. Membr. Sci*. **1983**, *13*, 307–326.

(10) Miyatake, K.; Chikashige, Y.; Watanabe, M. Tuned Polymer Electrolyte Membranes Based on Aromatic Polyethers for Fuel Cell Applications. *J. Am. Chem. Soc.,* **2007**, *129,* 3879–3887.

(11) Bae, B.; Miyatake, K.; Watanabe, M. Sulfonated Poly(arylene ether sulfone ketone) Multiblock Copolymers with Highly Sulfonated Block. Synthesis and Properties. *Macromolecules* **2010**, *43*, 2684–2691.

(12) Wang, C.; Li, N.; Shin, D. W.; Lee, S. Y.; Kang, N. R.; Lee, Y. M.; Guiver, M. D. Fluorene-Based Poly(arylene ether sulfone)s Containing Clustered Flexible Pendant Sulfonic Acids as Proton Exchange Membranes *Macromolecules* **2011**, *44*, 7296–7306.

(13) Li, N.; Wang, C.; Lee, S. Y.; Park, C. H.; Lee, Y. M.; Guiver, M. D. Enhancement of Proton Transport by Nanochannels in Comb-Shaped Copoly(Arylene Ether Sulfone)s *Angew. Chem., Int. Ed.* **2011**, *50*, 9158–9161.

(14) Chang, Y.; Brunello, G. F.; Fuller, J.; Hawley, M.;Kim, Y. S. Disabb-Miller, M.; Hickner, M. A.; Jang, S. S.; Bae, C. S. Aromatic Ionomers with Highly Acidic Sulfonate Groups: Acidity, Hydration, and Proton Conductivity. *Macromolecules* **2011**, *44*, 8458–8469.

(15) Chang, Y.; Mohanty, A. D.; Smedley, S. B.; Abu-Hakmeh, K.; Lee, Y. H.; Morgan, J. E.; Hickner, M. A.; Jang, S. S.; Ryu, C. Y.; Bae, C. Effect of Superacidic Side Chain Structures on High Conductivity Aromatic Polymer Fuel Cell Membranes. *Macromolecules* **2015**, *48*, 7117–7126.

(16) Nagao, Y. Proton Transport Property of Nafion Thin Films on MgO (100) with Anisotropic Molecular Structure. *e-J. Surf. Sci. Nanotechnol*. **2012**, *10,* 114–116.

(17) Nagao, Y. Highly Oriented Sulfonic Acid Groups in a Nafion Thin Film on Si Substrate. *J. Phys. Chem. C* **2013**, *117*, 3294–3297.

(18) Ono, Y.; Nagao, Y. Interfacial Structure and Proton Conductivity of Nafion at the Pt-Deposited Surface. *Langmuir* **2016**, *32*, 352–358.

(19) Sato, T.; Hayasaka, Y.; Mitsuishi, M.; Miyashita, T.; Nagano, S.; Matsui, J. High

Proton Conductivity in the Molecular Interlayer of a Polymer Nanosheet Multilayer Film. *Langmuir* **2015**, *31*, 5174–5180.

(20) Matsui, J.; Miyata, H.; Hanaoka, Y.; Miyashita, T. Layered Ultrathin Proton Conductive Film Based on Polymer Nanosheet Assembly. *ACS Appl. Mater. Interfaces* **2011**, *3* 1394–1397.

(21) Sato, T.; Tsukamoto, M.; Yamamoto, S.; Mitsuishi, M.; Miyashita, T.; Nagano, S.; Matsui Acid-Group-Content-Dependent Proton Conductivity Mechanisms at the Interlayer of Poly(N-dodecylacrylamide-co-acrylic acid) Copolymer Multilayer Nanosheet Films. *Langmuir* **2017**, *33*, 12897–12902.

(22) Krishnan, K.; Iwatsuki, H.; Hara, M.; Nagano, S.; Nagao, Y. Proton Conductivity Enhancement in Oriented, Sulfonated Polyimide Thin Films. *J. Mater. Chem. A* **2014**, *2*, 6895–6903.

(23) Krishnan, K.; Ymada, T.; Iwatsuki, H.; Hara, M.; Nagano, S.; Otsubo, K.; Sakata, A.; Kitagawa, H.; Nagao, Y. Influence of Confined Polymer Structure on Proton Transport Property in Sulfonated Polyimide Thin Films. *Electrochemistry* **2014**, *82*, 865–869.

(24) Krishnan, K.; Iwatsuki, H.; Hara, M.; Nagano, S.; Nagao, Y. Influence of Molecular Weight on Molecular Ordering and Proton Transport in Organized Sulfonated

Polyimide Thin Films. *J. Phys. Chem. C* **2015**, *119*, 21767–21774.

(25) Yabu, H.; Matsui, J.; Hara, M.; Nagano, S.; Matsuo, Y.; Nagao, Y. Proton Conductivities of Lamellae-Forming Bioinspired Block Copolymer Thin Films Containing Silver Nanoparticles. *Langmuir* **2016**, *32,* 9484–9491.

(26) Kongkanand, A. Interfacial Water Transport Measurements in Nafion Thin Films Using a Quartz-Crystal Microbalance. *J. Phys. Chem. C* **2011**, *115*, 11318–11325.

(27) Holdcroft, S. Fuel Cell Catalyst Layers: A Polymer Science Perspective. *Chem. Mater.* **2014**, *26*, 381–393.

(28) Paul, D. K.; Karan, K.; Docoslis, A.; Giorgi, J. B.; Pearce, J. Characteristics of Self-Assembled Ultrathin Nafion Films. *Macromolecules* **2013**, *46*, 3461–3475.

(29) Paul, D. K.; Fraser, A.; Karan, K. Towards the Understanding of Proton Conduction Mechanism in PEMFC Catalyst Layer: Conductivity of Adsorbed Nafion Films. *Electrochem. Commun.* **2011**, *13*, 774–777.

(30) Paul, D. K.; Karan, K. Conductivity and Wettability Changes of Ultrathin Nafion Films Subjected to Thermal Annealing and Liquid Water Exposure. *J. Phys. Chem. C* **2014**, *118*, 1828–1835.

(31) Dura, J. A.; Murthi, V. S.; Hartman, M.; Satija, S.; Majkrzak, C. F. Multilamellar Interface Structures in Nafion. *Macromolecules* **2009**, *42*, 4769–4774.

(32) Ogata, Y.; Kawaguchi, D.; Yamada, N. L.; Tanaka, K. Multistep Thickening of Nafion Thin Films in Water. *ACS Macro Lett.* **2013**, *2*, 856–859.

(33) Bass, M.; Berman, A.; Singh, A.; Konovalov, O.; Freger, V. Surface-Induced Micelle Orientation in Nafion Films. *Macromolecules* **2011**, *44*, 2893–2899.

(34) Modestino, M. A.; Paul, D. K.; Dishari, S.; Petrina, S. A.; Allen, F.; Hickner, M. A.; Karan, K.; Segalman, R. A.; Weber, A. Z. Self-Assembly and Transport Limitations in Confined Nafion Films. *Macromolecules* **2013**, *46*, 867–873.

(35) Shim, H. K.; Paul, D. K.; Karan, K. Resolving the Contradiction between Anomalously High Water Uptake and Low Conductivity of Nanothin Nafion films on SiO_2 Substrate. *Macromolecules* **2015**, *48*, 8394–8397.

(36) Kusoglu, A.; Kushner, D.; Paul, D. K.; Karan, K.; Hickner, M. A.; Weber, A. Z. Impact of Substrate and Processing on Confinement of Nafion Thin Films. *Adv. Funct. Mater.* **2014**, *24*, 4763–4774.

(37) Eastman, S. A.; Kim, S.; Page, K. A.; Rowe, B. W.; Kang, S.; Soles, C. L.; Yager, K. G. Effect of Confinement on Structure, Water Solubility, and Water Transport in Nafion Thin Films. *Macromolecules* **2012**, *45*, 7920–7930.

(38) Nagao, Y. Proton-Conductivity Enhancement in Polymer Thin Films. *Langmuir*, **2017**, *33* 12547–12558.

(39) Nagao, Y.; Krishnan, K.; Goto, R.; Hara, M.; Nagano, S. Effect of Casting Solvent on Interfacial Molecular Structure and Proton Transport Characteristics of Sulfonated Polyimide Thin Films. *Anal. Sci.* **2017**, *33*, 35–39.

(40) Soberats, B.; Yoshio, M.; Ichikawa, T.; Taguchi, S.; Ohno, H.; Kato, T. 3D Anhydrous Proton-Transporting Nanochannels Formed by Self-Assembly of Liquid Crystals Composed of a Sulfobetaine and a Sulfonic Acid. *J. Am. Chem. Soc.* **2013**, *135*, 15286–15289.

(41) Ichikawa, T.; Kato, T.; Ohno, H. 3D Continuous Water Nanosheet as a Gyroid Minimal Surface Formed by Bicontinuous Cubic Liquid-Crystalline Zwitterions. *J. Am. Chem. Soc.* **2012**, *134*, 11354–11357.

(42) Soberats, B.; Yoshio, M.; Ichikawa, T.; Zeng, X.; Ohno, H.; Ungar, G.; Kato, T. Ionic Switch Induced by a Rectangular-Hexagonal Phase Transition in Benzenammonium Columnar Liquid Crystals. *J. Am. Chem. Soc.* **2015**, *137*, 13212– 13215.

(43) Soberats, B.; Uchida, E.; Yoshio, M.; Kagimoto, J.; Ohno, H.; Kato, T. Macroscopic Photocontrol of Ion-Transporting Pathways of a Nanostructured Imidazolium-Based Photoresponsive Liquid Crystal. *J. Am. Chem. Soc.* **2014**, *136* 9552–9555.

(44) Hernandez, J.; Zhang, H.; Chen, Y.; Rosenthal, M.; Lingwood, M.; Goswami, M.; Zhu, X.; Moeller, M.; Madsen, L.; Ivanov, D. Bottom-Up Fabrication of

Nanostructured Bicontinuous and Hexagonal Ion-Conducting Polymer Membranes. *Macromolecules* **2017**, *50*, 5392–5401.

(45) Yoshio, M.; Kagata, T.; Hoshino, K.; Mukai, T.; Ohno, H.; Kato, T. One-Dimensional Ion-Conductive Polymer Films: Alignment and Fixation of Ionic Channels Formed by Self-Organization of Polymerizable Columnar Liquid Crystals. *J. Am. Chem. Soc.* **2006**, *128*, 5570–5577.

(46) Sakuda, J.; Hosono, E.; Yoshio, M.; Ichikawa, T.; Matsumoto, T.; Ohno, H.; Zhou, H.; Kato, T. Liquid-Crystalline Electrolytes for Lithium-Ion Batteries: Ordered Assemblies of a Mesogen-Containing Carbonate and a Lithium Salt. *Adv. Funct. Mater.* **2015**, *25*, 1206–1212.

(47) Ichikawa, T.; Kato, T.; Ohno, H. 3D Continuous Water Nanosheet as a Gyroid Minimal Surface Formed by Bicontinuous Cubic Liquid-Crystalline Zwitterions. *J. Am. Chem. Soc.* **2012**, *134*, 11354–11357.

(48) Soberats, B.; Yoshio, M.; Ichikawa, T.; Taguchi, S.; Ohno, H.; Kato, T. 3D Anhydrous Proton-Transporting Nanochannels Formed by Self-Assembly of Liquid Crystals Composed of a Sulfobetaine and a Sulfonic Acid. *J. Am. Chem. Soc.* **2013**, *135*, 15286–15289.

(49) Ichikawa, T.; Yoshio, M.; Hamasaki, A.; Taguchi, S.; Liu, F.; Zeng, X.; Ungar, G.;

Ohno, H.; Kato, T. Induction of Thermotropic Bicontinuous Cubic Phases in Liquid-Crystalline Ammonium and Phosphonium Salts. *J. Am. Chem. Soc.* **2012**, *134* 2634–2643.

(50) Wakita, J.; Jin, S.; Shin, T. J.; Ree, M.; Ando, S. Analysis of Molecular Aggregation Structures of Fully Aromatic and Semialiphatic Polyimide Films with Synchrotron Grazing Incidence Wide-Angle X-ray Scattering. *Macromolecules* **2010**, *43*, 1930–1941.

(51) Hasegawa, T. A Novel Measurement Technique of Pure Out-of-plane Vibrational Modes in Thin Films on a Nonmetallic Material with No Polarizer. *J. Phys. Chem. B* **2002**, *106*, 4112–4115.

(52) Hasegawa, T.; Matsumoto, L.; Kitamura, S.; Amino, S.; Katada, S.; Nishijo, J. Optimum Condition of Fourier Transform Infrared Multiple-Angle Incidence Resolution Spectrometry for Surface Analysis. *Anal. Chem*. **2002**, *74*, 6049–6054.

(53)Hasegawa, T. Advanced Multiple-angle Incidence Resolution Spectrometry for Thin-layer Analysis on a Low-refractive-index Substrate. *Anal. Chem.* **2007**, *79*, 4385–4389.

(54)Hasegawa, T.; Itoh, Y.; Kasuya, A. A. Experimental Optimization of P-polarized MAIR Spectrometry Performed on a Fourier Transform Infrared Spectrometer. *Anal. Sci*. **2008**, *24*, 105–109.

For Table of Contents Use Only